

Analysis of pitchfork bifurcations and symmetry breaking in the elliptic restricted three-body problem

Haozhe Shu^{1,2} and Mingpei Lin^{*1}

¹*Advanced Institute for Material Research, Tohoku University, Sendai, 980-8577, Japan*

²*Mathematical Institute, Tohoku University, Sendai, 980-8578, Japan*

A unified framework is proposed to quantitatively characterize pitchfork bifurcations and associated symmetry breaking in the elliptic restricted three-body problem (ERTBP). It is known that planar/vertical Lyapunov orbits and Lissajous orbits near the collinear libration points undergo pitchfork bifurcations with varying orbital energy. These bifurcations induce symmetry breaking, generating bifurcated families including halo/quasi-halo orbits, axial/quasi-axial orbits, and their corresponding invariant manifolds. Traditional semi-analytical methods for constructing halo orbits, based on resonant bifurcation mechanisms, have obstacles in fully exploiting the intrinsic symmetry breaking characteristics in pitchfork bifurcations. In this paper, we propose a unified trigonometric series-based framework to analyze these bifurcated families from the perspective of coupling-induced bifurcation mechanisms. By introducing a coupling coefficient and various bifurcation equations into the ERTBP, different symmetry breaking is achieved when the coupling coefficient is non-zero. This unified semi-analytical framework captures bifurcations of both periodic/quasi-periodic and transit/non-transit orbits. Furthermore, it reveals that pitchfork bifurcation solutions in the ERTBP fundamentally depend solely on the orbital eccentricity and three amplitude parameters of the system's degrees of freedom, governing both the elliptic direction and the hyperbolic one.

Keywords: Elliptic restricted three-body problem, Pitchfork bifurcation, Symmetry breaking, Coupling-induced bifurcation mechanism, Libration point orbit

I. Introduction

The spatial circular restricted three-body problem (CRTBP), which describes the motion of an infinitesimal body (spacecraft or asteroid) under the gravitational influence of two primaries in circular orbits, serves as a foundational model in celestial mechanics [1, 2]. As a first natural extension, the elliptic restricted three-body problem (ERTBP) generalizes this framework by allowing the primaries to evolve along small-eccentricity Keplerian orbits. The ERTBP

*Corresponding author: lin.mingpei.d2@tohoku.ac.jp

introduces explicit time dependence and results in the absence of a first integral [3, 4]. This modification transforms the five stationary Lagrangian points in CRTBP into "instantaneous equilibrium positions" with periodic oscillations. Compared to the corresponding CRTBP, the ERTBP provides a more precise and essential framework for modeling real-world celestial systems, particularly in scenarios involving planetary resonances, asteroid dynamics, and planet-moon systems [5]. Deep insights into these dynamical structures also enable optimized spacecraft trajectories, including libration point orbit transfers [6, 7], station-keeping strategies [8, 9], and resonant flyby for deep-space exploration [10].

The dynamics near the collinear libration points in the restricted three-body problem (RTBP) have been extensively studied through both numerical and analytical approaches. For numerical perspectives, Peng et al. [11] generated multi-revolution halo orbits via continuation methods and multi-segments optimization methods. Initializing with periodic orbits in the CRTBP, Ferrari et al. [12] succeeded in finding periodic orbits in the ERTBP through a differential correction algorithm. Paez et al. [13] classified transit orbits in the ERTBP through the Floquet-Birkhoff normalization approach. Recently, Jorba et al. [14] systematically analyzed Hilda asteroids, which are related to a 3:2 orbital resonance with Jupiter and provided a comparison work between the CRTBP and the ERTBP.

For analytical perspectives, high-precision orbit approximations are essential for characterizing local dynamics, offering both physical insights and initial guesses for numerical methods. To derive approximate high-order analytical solutions, two prominent techniques have been developed: the Lindstedt-Poincaré perturbation method and the Hamiltonian normal form method. Farquhar [15] pioneered the concept of halo orbits using a frequency control scheme. Building on this foundation, 1:1 resonant bifurcation mechanisms were developed to systematically obtain halo families semi-analytically. Based on the synchronization construction of the in-plane and out-of-plane oscillators, Richardson [16] constructed a third-order analytical solution for halo orbits by incorporating a correction term to adjust the out-of-plane frequency. Further advancement was made by Masdemont [17], who derived high-order series solutions for invariant manifolds in the CRTBP.

In contrast to the Lindstedt-Poincaré method, the Hamiltonian normal form offers a distinct yet powerful approach for analyzing the local dynamics. Within this framework, Jarba and Masdemont. [18] obtained a qualitative description of the local phase space by analyzing the reduced Hamiltonian in the CRTBP. Paez and Guzzo [19] presented a semi-analytical construction of halo orbits and halo tubes in the elliptic model using the Floquet-Birkhoff resonant normal form. In the most recent, based on the Lie transform, Celletti and Lhotka et al. [20] presented an explicit resonant normal form, enabling analytical investigations of planar/vertical Lyapunov orbits and halo orbits in the ERTBP.

Even though, based on the resonant framework, the first-level bifurcations associated with periodic orbits have been thoroughly analyzed by using semi-analytical approaches, the indirect relationship between 1:1 resonant bifurcation mechanisms and potential bifurcations associated with quasi-periodic orbits and transit/non-transit orbits motivates some other insights. Lin et al. [21, 22] initially addressed coupling-induced mechanisms in the CRTBP. Without

relying on the classical constructions of resonant modification, a so-called coupling modification was comparably introduced to finally obtain a comprehensive semi-analytical construction of the local phase space in the CRTBP.

In this paper, we present a systematic analysis of pitchfork bifurcations and associated symmetry breaking near the collinear libration points in the ERTBP, within a unified trigonometric series-based framework. Known as a three degree-of-freedom (DOF) non-autonomous Hamiltonian system, the governing differential equations of the ERTBP totally exhibit three distinct types of symmetries. Pitchfork bifurcations arise near the collinear libration points, accompanied by the breaking of certain characteristic symmetries in the non-bifurcated solutions [23]. To achieve the corresponding symmetry breaking from non-bifurcated solutions, we introduce bifurcation equations and coupling coefficients along specific directions in the dynamical model of the ERTBP, by using coupling-induced mechanisms. These coefficients are derived by solving the coupled bifurcation equations, while non-zero coupling coefficients lead to symmetry breaking in the original solutions. This symmetry breaking subsequently triggers pitchfork bifurcations. To fully utilize the symmetries of the ERTBP, the hyperbolic part of the solution is also formulated in a triangular form defined on the complex plane, which completes a unified trigonometric form in the series expansions of general solutions. In addition to the bifurcation analysis associated with center manifolds, the analysis of the constructed bifurcation equation also provides deep insights into the bifurcation of the transit/non-transit orbits. All types of bifurcated solutions in the form of trigonometric series are shown to depend solely on the eccentricity and three amplitudes corresponding to the system's DOFs, where the critical conditions are derived explicitly.

The remainder of the paper is organized as follows. In Section 2, the dynamic model of the ERTBP is introduced in a pulsating-rotating frame. In Section 3, we present a unified trigonometric series-based semi-analytical construction for the bifurcated orbits. A quantitative analysis of pitchfork bifurcations and symmetry breaking is proposed in Section 4. Finally, Section 5 offers conclusions.

II. Dynamic model

In this section, the dynamic model of the ERTBP is introduced. The model describes the motion of an infinitesimal particle in the gravitational field of two primaries. By neglecting the attraction influence of the particle on the primaries, the motion of two primaries can be described by the Kepler orbits around their common centroid. The classical pulsating-rotating frame is employed to simplify the formulation of the dynamical model. Specifically, positioning the origin at the centroid of the two primaries, the orientation of the X -axis is given by the line that goes from the smaller primary to the larger primary, while the Z -axis has the orientation determined by the angular motion of the primaries. Y -axis completes the right-handed coordinate system. In this case, the normalized coordinates for the smaller and the larger primary are $(1 - \mu, 0, 0)$ and $(\mu, 0, 0)$ respectively, where $\mu = m_2/(m_1 + m_2)$ is the system parameter, representing the mass ratio of the smaller celestial body to the sum of the masses of the two bodies. The governing differential equations describing the motion of the infinitesimal particle in the normalized pulsating-synodic

frame are as follows [6]:

$$\begin{aligned} X'' - 2Y' &= \frac{\partial \Omega}{\partial X}, \\ Y'' + 2X' &= \frac{\partial \Omega}{\partial Y}, \\ Z'' &= \frac{\partial \Omega}{\partial Z}, \end{aligned} \quad (1)$$

where

$$\Omega(X, Y, Z, f) = \frac{1}{1 + e \cos f} \left[\frac{1}{2}(X^2 + Y^2) + \frac{1 - \mu}{r_1} + \frac{\mu}{r_2} + \frac{1}{2}\mu(1 - \mu) \right]$$

represents the potential in the ERTBP. Here, e is orbital eccentricity and f represents the true anomaly of the secondary on the elliptic orbit. The derivatives of coordinate are defined as

$$X' := \frac{dX}{df}, \quad Y' := \frac{dY}{df}, \quad Z' := \frac{dZ}{df}.$$

r_1 and r_2 denote the instantaneous distance from the spacecraft to the massive and secondary primaries, satisfying

$$\begin{aligned} r_1^2 &= (X - \mu)^2 + Y^2 + Z^2, \\ r_2^2 &= (X + 1 - \mu)^2 + Y^2 + Z^2. \end{aligned} \quad (2)$$

The non-autonomous nature of governing equations of the ERTBP introduces complicated time-dependent perturbations. When the eccentricity $e = 0$, this dynamical model reduces to the well-known autonomous CRTBP. Similar to the CRTBP, the ERTBP (1) possesses three kinds of symmetries given by [23]:

$$\begin{aligned} S_1 &: (f, X, Y, Z, X', Y', Z') \longleftrightarrow (f, X, Y, -Z, X', Y', -Z'), \\ S_2 &: (f, X, Y, Z, X', Y', Z') \longleftrightarrow (-f, X, -Y, Z, -X', Y', -Z'), \\ S_3 &: (f, X, Y, Z, X', Y', Z') \longleftrightarrow (-f, X, -Y, -Z, -X', Y', Z'). \end{aligned} \quad (3)$$

For instance, suppose that a curve $(X(f), Y(f), Z(f))$ solves (1). It's clear that its reflection about the (X, Y) plane, $(X(f), Y(f), -Z(f))$ is also a solution to (1). Moreover, after time reversal, its reflection about the (X, Z) plane, $(X(-f), -Y(-f), Z(-f))$, also satisfies the governing differential equations. In (1), there are five Lagrange points pulsating in the synodic coordinate system. Three of these are collinear libration points, while the remaining two are triangular libration points. Inheriting the notation in the CRTBP, we denote the collinear libration points by L_i ($i = 1, 2, 3$). By adopting the following transformations of coordinates reference, the origin of the original

normalized synodic coordinate system can be relocated to the collinear libration points:

$$\begin{aligned} X &= -\gamma_i x + \mu - 1 + \gamma_i, Y = -\gamma_i y, Z = \gamma_i z, i = 1, 2; \\ X &= \gamma_i x + \mu + \gamma_i, Y = \gamma_i y, Z = \gamma_i z, i = 3, \end{aligned} \quad (4)$$

with γ_i denoting the instantaneous distance between the libration point L_i and its closest primary. It's known that the value of γ_i are determined by the unique positive root of Euler's quintic equation [18, 24]:

$$\begin{aligned} \gamma_i^5 \mp (3 - \mu)\gamma_i^4 + (3 - 2\mu)\gamma_i^3 - \mu\gamma_i^2 \pm 2\mu\gamma_i - \mu &= 0, i = 1, 2; \\ \gamma_i^5 + (2 + \mu)\gamma_i^4 + (1 + 2\mu)\gamma_i^3 - (1 - \mu)\gamma_i^2 - 2(1 - \mu)\gamma_i - (1 - \mu) &= 0, i = 3, \end{aligned} \quad (5)$$

where the upper and lower signs correspond to L_1 and L_2 , respectively. In the transformed coordinate system, the governing equations (1) become

$$\begin{aligned} x'' - 2y' &= \frac{\partial \Omega}{\partial x}, \\ y'' + 2x' &= \frac{\partial \Omega}{\partial y}, \\ z'' &= \frac{\partial \Omega}{\partial z}, \end{aligned} \quad (6)$$

with

$$\Omega(x, y, z, f) = \frac{1}{1 + e \cos f} \left[\frac{1}{2} ((\mu - 1 \mp \gamma(x - 1))^2 + \gamma^2 y^2) + \frac{1 - \mu}{r_1} + \frac{\mu}{r_2} + \frac{1}{2} \mu (1 - \mu) \right].$$

To obtain a high-order semi-analytical construction for bifurcated orbits near the collinear libration points, the right-hand side of (6) is expanded into a recurrent form [17]:

$$\begin{aligned} x'' - 2y' - (1 + 2c_2)x &= \sum_{i \geq 1} [(1 + 2c_2)x(-e)^i \cos^i f] \\ &+ \sum_{i \geq 0} \{(-e)^i \cos^i f [\sum_{n \geq 2} c_{n+1}(n+1)T_n(x, y, z)]\}, \\ y'' + 2x' + (c_2 - 1)y &= \sum_{i \geq 1} [(1 - c_2)y(-e)^i \cos^i f] \\ &+ \sum_{i \geq 0} \{(-e)^i \cos^i f [y \sum_{n \geq 2} c_{n+1}R_{n-1}(x, y, z)]\}, \\ z'' + c_2 z &= \sum_{i \geq 1} [-c_2 z(-e)^i \cos^i f] \\ &+ \sum_{i \geq 0} \{(-e)^i \cos^i f [z \sum_{n \geq 2} c_{n+1}R_{n-1}(x, y, z)]\}. \end{aligned} \quad (7)$$

Here, $\{T_n\}$ and $\{R_n\}$ are sequences of homogeneous polynomials defined by the recurrence relations

$$T_n = \frac{2n-1}{n}xT_{n-1} - \frac{n-1}{n}(x^2 + y^2 + z^2)T_{n-2}, \quad n \geq 2, \quad (8)$$

with initial states $T_0 = 1$, $T_1 = x$ and

$$R_n = \frac{2n+3}{n+2}xR_{n-1} - \frac{2n+2}{n+2}T_n - \frac{n+1}{n+2}(x^2 + y^2 + z^2)R_{n-2}, \quad n \geq 2, \quad (9)$$

with initial states $R_0 = -1$, $R_1 = -3x$. The coefficients c_n depend solely on the system parameter μ and are given by

$$\begin{aligned} c_n(\mu) &= \frac{1}{\gamma_i^3} [(\pm 1)^n \mu + (-1)^n \frac{(1-\mu)\gamma_i^{n+1}}{(1 \mp \gamma_i)^{n+1}}], \quad \text{for } L_i, \quad i = 1, 2; \\ c_n(\mu) &= \frac{(-1)^n}{\gamma_i^3} [1 - \mu + \frac{\mu\gamma_i^{n+1}}{(1 + \gamma_i)^{n+1}}], \quad \text{for } L_i, \quad i = 3. \end{aligned} \quad (10)$$

III. Semi-analytical construction of bifurcated families in the ERTBP

In this section, we introduce a coupling coefficient and several bifurcation equations in the ERTBP. Based on different coupling directions, linear solutions are modified correspondingly. Initializing with these modified solutions, we develop a unified trigonometric series-based framework to iteratively construct a semi-analytical solution for describing the phase space near collinear libration points. By comprehensively considering all three cases of coupling constructions, the bifurcated orbits associated with the breaking of both S_1 -type and S_2 -type symmetries are approximated using modified high-order series expansions.

A. Modified perturbation procedure

The linearized equations associated with the ERTBP model (7) are given by

$$\begin{aligned} x'' - 2y' - (1 + 2c_2)x &= \sum_{i \geq 1} [(1 + 2c_2)x(-e)^i \cos^i f], \\ y'' + 2x' + (c_2 - 1)y &= \sum_{i \geq 1} [(1 - c_2)y(-e)^i \cos^i f], \\ z'' + c_2z &= \sum_{i \geq 1} [(1 - c_2)z(-e)^i \cos^i f], \end{aligned} \quad (11)$$

Here, to obtain an explicit linear solution used in the initialization of the Lindstedt-Poincaré method, we start with the autonomous linear counterpart of (11), given by

$$\begin{aligned}
x'' - 2y' - (1 + 2c_2)x &= 0, \\
y'' + 2x' + (c_2 - 1)y &= 0, \\
z'' + c_2z &= 0.
\end{aligned} \tag{12}$$

The first-order solution of (12) can be explicitly expressed as

$$\begin{aligned}
x(f) &= \alpha_1 \cos \theta_1 + \alpha_3 \cos \theta_3, \\
y(f) &= \kappa_1 \alpha_1 \sin \theta_1 + \sqrt{-1} \kappa_2 \alpha_3 \sin \theta_3, \\
z(f) &= \alpha_2 \cos \theta_2,
\end{aligned} \tag{13}$$

where $\alpha_1, \alpha_2 \in \mathbb{R}$, $\alpha_3 \in \sqrt{-1}\mathbb{R} \cup \mathbb{R}$, $\theta_1 = \omega_0 f + \varphi_1$, $\theta_2 = \nu_0 f + \varphi_2$, and $\theta_3 = \sqrt{-1} \lambda_0 f + \varphi_3$, satisfying that

$$\begin{aligned}
\omega_0 &= \sqrt{\frac{2 - c_2 + \sqrt{9c_2^2 - 8c_2}}{2}}, \quad \nu_0 = \sqrt{c_2}, \quad \lambda_0 = \sqrt{\frac{c_2 - 2 + \sqrt{9c_2^2 - 8c_2}}{2}}, \\
\kappa_1 &= -\frac{\omega_0^2 + 2c_2 + 1}{2\omega_0}, \quad \kappa_2 = -\frac{\lambda_0^2 - 2c_2 - 1}{2\lambda_0}.
\end{aligned}$$

Here, α_1 and α_2 represent the in-plane and out-of-plane amplitudes associated with the center part of the solution, respectively, while α_3 corresponds to the amplitude associated with the hyperbolic part. φ_i ($i = 1, 2, 3$) are the three corresponding initial phase angles. The coefficients κ_1 and κ_2 depend solely on the mass parameters of the RTBP. It is noted that the hyperbolic part in (13) is also expressed in a trigonometric form with complex amplitude and phase. The solution with amplitude α_3 lying on the real axis describes the motion of non-transit orbit, while the imaginary-valued α_3 corresponds to the transit motion.

Along the family of planar Lyapunov orbits around collinear libration points, a pitchfork bifurcation occurs when the North-South symmetry (the S_1 -type symmetry in (3)) of the solution is broken. The resulting bifurcated periodic orbits are known as halo orbits. To characterize this bifurcation, we consider a coupling effect from the motion in the

x -direction to the z -direction in (7). The modified equation of motion is expressed as:

$$\begin{aligned}
x'' - 2y' - (1 + 2c_2)x &= \sum_{i \geq 1} [(1 + 2c_2)x(-e)^i \cos^i f] \\
&\quad + \sum_{i \geq 0} \{(-e)^i \cos^i f [\sum_{n \geq 2} c_{n+1}(n+1)T_n(x, y, z)]\}, \\
y'' + 2x' + (c_2 - 1)y &= \sum_{i \geq 1} [(1 - c_2)y(-e)^i \cos^i f] \\
&\quad + \sum_{i \geq 0} \{(-e)^i \cos^i f [y \sum_{n \geq 2} c_{n+1}R_{n-1}(x, y, z)]\}, \\
z'' + c_2z &= \sum_{i \geq 1} [-c_2z(-e)^i \cos^i f] \\
&\quad + \sum_{i \geq 0} \{(-e)^i \cos^i f [z \sum_{n \geq 2} c_{n+1}R_{n-1}(x, y, z)]\} + \eta \Delta x,
\end{aligned} \tag{14}$$

where η is called the coupling coefficient and Δ represents the correction factor satisfying a bifurcation equation $\Delta = 0$, which will be discussed later. By linearizing (14), we obtain a modified linear equation, given by

$$\begin{aligned}
x'' - 2y' - (1 + 2c_2)x &= 0, \\
y'' + 2x' + (c_2 - 1)y &= 0, \\
z'' + c_2z &= \eta d_{0000}x.
\end{aligned} \tag{15}$$

By solving (15), the modified linear solution is expressed as

$$\begin{aligned}
x(f) &= \alpha_1 \cos \theta_1 + \alpha_3 \cos \theta_3, \\
y(f) &= \kappa_1 \alpha_1 \sin \theta_1 + \sqrt{-1} \kappa_2 \alpha_3 \sin \theta_3, \\
z(f) &= \alpha_2 \cos \theta_2 + \eta \alpha_1 \cos \theta_1 + \eta \kappa_3 \alpha_3 \cos \theta_3,
\end{aligned} \tag{16}$$

where $\kappa_3 = \frac{\nu_0^2 - \omega_0^2}{\nu_0^2 + \lambda_0^2}$, $d_{0000} = \nu_0^2 - \omega_0^2$.

When considering the perturbations of both nonlinear terms and orbital eccentricity, the high-order solution around collinear libration points in the ERTBP can be expressed as a formal expansion in powers of three amplitude parameters, and the orbital eccentricity:

$$\begin{aligned}
x(f) &= \sum x_{ijkm}^{stur} \cos(s\theta_1 + t\theta_2 + u\theta_3 + rf) \alpha_1^i \alpha_2^j \alpha_3^k e^m, \\
y(f) &= \sum y_{ijkm}^{stur} \sin(s\theta_1 + t\theta_2 + u\theta_3 + rf) \alpha_1^i \alpha_2^j \alpha_3^k e^m, \\
z(f) &= \sum z_{ijkm}^{stur} \cos(s\theta_1 + t\theta_2 + u\theta_3 + rf) \alpha_1^i \alpha_2^j \alpha_3^k e^m,
\end{aligned} \tag{17}$$

where $\theta_1 = \omega f + \varphi_1$, $\theta_2 = \nu f + \varphi_2$, and $\theta_3 = \sqrt{-1}\lambda f + \varphi_3$. Furthermore, the motion frequencies are not constant during the perturbation procedure and depend on the amplitudes α_i and the eccentricity e . Therefore, they are expressed as power series:

$$\begin{aligned}\omega &= \sum \omega_{ijkm} \alpha_1^i \alpha_2^j \alpha_3^k e^m, \\ \nu &= \sum \nu_{ijkm} \alpha_1^i \alpha_2^j \alpha_3^k e^m, \\ \lambda &= \sum \lambda_{ijkm} \alpha_1^i \alpha_2^j \alpha_3^k e^m.\end{aligned}\tag{18}$$

Likewise, the defined correction term Δ is expanded as $\Delta = \sum d_{ijkm} \alpha_1^i \alpha_2^j \alpha_3^k e^m$. To ensure that (17) is a valid solution of the original equation (7), the constraint condition $\eta\Delta = 0$ must be satisfied. Here, $\Delta = 0$ establishes an implicit relationship between the amplitudes α_i ($i = 1, 2, 3$), the orbital eccentricity e , and the coupling coefficient η . For any choice of the quartet $(\alpha_1, \alpha_2, \alpha_3, e)$, if there exist some $\eta \neq 0$ satisfying the polynomial bifurcation equation $\Delta = 0$, it indicates the occurrence of a bifurcation. Conversely, no bifurcation occurs if $\eta = 0$. In this case, the high-order computation of planar/vertical Lyapunov orbits and Lissajous orbits and the corresponding transit/non-transit orbits can be derived. Since the iterative process is initialized with the modified linear solution (16), it is clear to see:

$$\begin{aligned}\omega_{0000} &= \omega_0, \nu_{0000} = \nu_0, \lambda_{0000} = \lambda_0; \\ x_{1000}^{1000} &= x_{0010}^{0010} = 1, y_{1000}^{1000} = \kappa_1, y_{0010}^{0010} = \sqrt{-1}\kappa_2; \\ z_{1000}^{1000} &= \eta, z_{0100}^{0100} = 1, z_{0010}^{0010} = \eta\kappa_3.\end{aligned}$$

Similar to halo families, it is known that associated with the breaking of the S_2 -type symmetry in (3), the families of axial orbits bifurcate from both planar and vertical Lyapunov orbits. Each axial family consists of two branches related by the reflection across the (x, y) plane. To illustrate this, a similar algorithm for the high-order computation of axial/quasi-axial orbits and their corresponding transit and non-transit orbits can be derived by introducing a coupling effect between the z -directional motion and the motion in the y -direction. Here, we can obtain the following two kinds of modified dynamical models. For the first case, where the motion in the y -direction is coupled to the motion in the

z-direction, the governing differential equations are reformulated as

$$\begin{aligned}
x'' - 2y' - (1 + 2c_2)x &= \sum_{i \geq 1} [(1 + 2c_2)x(-e)^i \cos^i f] \\
&\quad + \sum_{i \geq 0} \{(-e)^i \cos^i f [\sum_{n \geq 2} c_{n+1}(n+1)T_n(x, y, z)]\}, \\
y'' + 2x' + (c_2 - 1)y &= \sum_{i \geq 1} [(1 - c_2)y(-e)^i \cos^i f] \\
&\quad + \sum_{i \geq 0} \{(-e)^i \cos^i f [y \sum_{n \geq 2} c_{n+1}R_{n-1}(x, y, z)]\}, \\
z'' + c_2z &= \sum_{i \geq 1} [-c_2z(-e)^i \cos^i f] \\
&\quad + \sum_{i \geq 0} \{(-e)^i \cos^i f [z \sum_{n \geq 2} c_{n+1}R_{n-1}(x, y, z)]\} + \eta \Delta y,
\end{aligned} \tag{19}$$

with the modified linear solution used to initialize the perturbation procedure given by

$$\begin{aligned}
x(t) &= \alpha_1 \cos(\omega_0 t + \varphi_1) + \alpha_3 \cos(\sqrt{-1}\lambda_0 t + \varphi_3), \\
y(t) &= \kappa_1 \alpha_1 \sin(\omega_0 t + \varphi_1) + \sqrt{-1}\kappa_2 \alpha_3 \sin(\sqrt{-1}\lambda_0 t + \varphi_3), \\
z(t) &= \alpha_2 \sin(\nu_0 t + \varphi_2) + \eta \alpha_1 \sin(\omega_0 t + \varphi_1) + \sqrt{-1}\eta \kappa_3 \alpha_3 \sin(\sqrt{-1}\lambda_0 t + \varphi_3),
\end{aligned} \tag{20}$$

where $d_{0000} = (\nu_0^2 - \omega_0^2)/\kappa_1$, $\kappa_3 = \frac{\kappa_2}{\kappa_1} \frac{\nu_0^2 - \omega_0^2}{\nu_0^2 + \lambda_0^2}$. For the second case, where the motion in the z-direction is coupled to the motion in the y-direction, the dynamical model is given by

$$\begin{aligned}
x'' - 2y' - (1 + 2c_2)x &= \sum_{i \geq 1} [(1 + 2c_2)x(-e)^i \cos^i f] \\
&\quad + \sum_{i \geq 0} \{(-e)^i \cos^i f [\sum_{n \geq 2} c_{n+1}(n+1)T_n(x, y, z)]\}, \\
y'' + 2x' + (c_2 - 1)y &= \sum_{i \geq 1} [(1 - c_2)y(-e)^i \cos^i f] \\
&\quad + \sum_{i \geq 0} \{(-e)^i \cos^i f [y \sum_{n \geq 2} c_{n+1}R_{n-1}(x, y, z)]\} + \eta \Delta z, \\
z'' + c_2z &= \sum_{i \geq 1} [-c_2z(-e)^i \cos^i f] \\
&\quad + \sum_{i \geq 0} \{(-e)^i \cos^i f [z \sum_{n \geq 2} c_{n+1}R_{n-1}(x, y, z)]\},
\end{aligned} \tag{21}$$

Table 1 Classification of types of coupling directions and their corresponding symmetry breaking

Type of symmetry breaking	Coupling direction	Type of bifurcated orbit
S_1	$x \rightarrow z$	Halo/quasi-halo orbits and their corresponding transit/non-transit orbits
S_2	$y \rightarrow z$ $z \rightarrow y$	Axial/quasi-axial orbits and their corresponding transit/non-transit orbits

with the corresponding modified linear solution expressed as

$$\begin{aligned}
 x(t) &= \alpha_1 \cos(\omega_0 t + \varphi_1) + \eta \alpha_2 \cos(\nu_0 t + \varphi_2) + \alpha_3 \cos(\sqrt{-1} \lambda_0 t + \varphi_3), \\
 y(t) &= \kappa_1 \alpha_1 \sin(\omega_0 t + \varphi_1) + \eta \kappa_3 \alpha_2 \sin(\nu_0 t + \varphi_2) + \sqrt{-1} \kappa_2 \alpha_3 \sin(\sqrt{-1} \lambda_0 t + \varphi_3), \\
 z(t) &= \alpha_2 \sin(\nu_0 t + \varphi_2),
 \end{aligned} \tag{22}$$

with $d_{0000} = \frac{1}{2\nu_0} - \frac{\nu_0}{2}$, $\kappa_3 = -\frac{1}{2\nu_0} - \frac{3\nu_0}{2}$. In both cases, the formal solution of the modified nonlinear dynamical model is expressed as

$$\begin{aligned}
 x(f) &= \sum x_{ijkm}^{stur} \cos(s\theta_1 + t\theta_2 + u\theta_3 + rf) \alpha_1^i \alpha_2^j \alpha_3^k e^m, \\
 y(f) &= \sum y_{ijkm}^{stur} \sin(s\theta_1 + t\theta_2 + u\theta_3 + rf) \alpha_1^i \alpha_2^j \alpha_3^k e^m, \\
 z(f) &= \sum z_{ijkm}^{stur} \sin(s\theta_1 + t\theta_2 + u\theta_3 + rf) \alpha_1^i \alpha_2^j \alpha_3^k e^m,
 \end{aligned} \tag{23}$$

while the expansions of the frequencies and the coupling correction term Δ retain the same formulations in (18).

In contrast to the conventional perturbation techniques that depend on the 1:1 resonant modification of the in-plane and out-of-plane frequencies, our approach establishes a unified trigonometric series-based framework, where coupling-induced bifurcation mechanisms are used for systematically achieving symmetry breaking in non-bifurcated solutions. The constructions of bifurcation equations according to different coupling effects are summarized with their associated symmetry breaking in Table 1.

Remark. It can be noticed that our analysis specifically addresses S_1 - and S_2 -type symmetry-breaking mechanisms, while S_3 -type is absent. In fact, S_3 -type symmetry is a combination of the first two, meaning that symmetry breaking occurs sequentially twice. Consequently, the orbits near collinear libration points may undergo two successive pitchfork bifurcations. From the global bifurcation diagram (Figure 3) of the CRTBP in [23], this bifurcation corresponds to the W_4 and W_5 families of orbits. The initial linear solutions for these orbits need to be obtained by incorporating corrections from two coupling-induced bifurcation equations. However, since the W_4 and W_5 families is significantly far from the collinear libration points, obtaining an accurate semi-analytical approximation of the W_4 and W_5 families using the local Lindstedt-Poincaré perturbation method remains challenging.

B. Computation of undetermined coefficients

1. Computation of the bifurcated orbits associating with the breaking of the S_1 -type symmetry

To obtain the semi-analytical computation up to finite order n , we need to determine the cosine coefficients x_{ijkm}^{stur} , z_{ijkm}^{stur} ; the sine coefficients y_{ijkm}^{stur} ; the coefficients for the three frequencies ω_{ijkm} , ν_{ijkm} , and λ_{ijkm} , as well as the coefficients d_{ijkm} in the bifurcation equation. Starting with the solution up to order $n - 1$ ($n \geq 2$), we substitute it into (14) to obtain all the known terms. These known terms are moved to the right-hand side of (14) and denoted by three new series p , q and τ . Specifically, their n -th order terms p_{ijkm}^{stur} , q_{ijkm}^{stur} , and τ_{ijkm}^{stur} with $i + j + k + m = n$ are fully determined. In this way, n -th order unknown coefficients can be obtained by solving a sequence of linear equations, where the unknown terms on the left-hand side match the known terms on the right-hand side in (14). Apart from three singular cases ($|i| + |j| + |k| = 1$), the general form of these linear equations is as follows:

$$\begin{bmatrix} -\tilde{\omega}_{stur}^2 - 1 - 2c_2 & -2\tilde{\omega}_{stur} \\ -2\tilde{\omega}_{stur} & -\tilde{\omega}_{stur}^2 + c_2 - 1 \end{bmatrix} \begin{bmatrix} x_{ijkm}^{stur} \\ y_{ijkm}^{stur} \end{bmatrix} = \begin{bmatrix} p_{ijkm}^{stur} \\ q_{ijkm}^{stur} \end{bmatrix}, \quad (24)$$

$$(c_2 - \tilde{\omega}_{stur}^2)z_{ijkm}^{stur} = \tau_{ijkm}^{stur} + \eta d_{0000} x_{ijkm}^{stur}, \quad (25)$$

where $\tilde{\omega}_{stur} = s\omega_0 + t\nu_0 + \sqrt{-1}u\lambda_0 + r$ is a complex-valued constant. Due to the definitions of ω_0 , ν_0 and λ_0 , the determinant of the coefficient matrix is non-zero. Hence, the undetermined coefficients in (24) and (25) can be solved directly. Nevertheless, when specific quartets (s, t, u, r) are selected, singularities emerge in the linear equation system. These exceptional cases include the following scenarios:

Case 1: $(s, t, u, r) = (1, 0, 0, 0)$.

In this case, the linear algebraic equations are formulated as

$$\begin{bmatrix} -\omega_0^2 - 1 - 2c_2 & -2\omega_0 \\ -2\omega_0 & -\omega_0^2 + c_2 - 1 \end{bmatrix} \begin{bmatrix} x_{ijkm}^{1000} \\ y_{ijkm}^{1000} \end{bmatrix} + \begin{bmatrix} -2(\kappa_1 + \omega_0)\omega_{i-1jkm} \\ -2(1 + \kappa_1\omega_0)\omega_{i-1jkm} \end{bmatrix} = \begin{bmatrix} p_{ijkm}^{1000} \\ q_{ijkm}^{1000} \end{bmatrix} + \begin{bmatrix} \Omega_{i-1jkm} \\ \kappa_1\Omega_{i-1jkm} \end{bmatrix}, \quad (26)$$

$$(c_2 - \omega_0^2)z_{ijkm}^{1000} - 2\eta\omega_0\omega_{i-1jkm} = \tau_{ijkm}^{1000} + \eta d_{0000} x_{ijkm}^{1000} + \eta d_{i-1jkm} + \eta\Omega_{i-1jkm}, \quad (27)$$

where $\Omega_{i-1jkm} = \omega^2 - 2\omega_0\omega_{i-1jkm}$ represents the corresponding known term of ω^2 of order $n - 1$. Equation (26) is singular. We set $x_{ijkm}^{1000} = 0$, and then, y_{ijkm}^{1000} and ω_{i-1jkm} can be obtained by dealing with the following reduced regular system of equations:

$$\begin{bmatrix} -2\omega_0 & -2(\kappa_1 + \omega_0) \\ -\omega_0^2 + c_2 - 1 & -2(1 + \kappa_1\omega_0) \end{bmatrix} \begin{bmatrix} y_{ijkm}^{1000} \\ \omega_{i-1jkm} \end{bmatrix} = \begin{bmatrix} p_{ijkm}^{1000} \\ q_{ijkm}^{1000} \end{bmatrix} + \begin{bmatrix} \Omega_{i-1jkm} \\ \kappa_1\Omega_{i-1jkm} \end{bmatrix}, \quad (28)$$

Similarly, by letting $z_{ijkm}^{1000} = 0$, the coefficients d_{i-1jkm} are solvable as well.

Case 2: $(s, t, u, r) = (0, 1, 0, 0)$.

The linear equations of the undetermined coefficients are as follows:

$$\begin{bmatrix} -v_0^2 - 1 - 2c_2 & -2v_0 \\ -2v_0 & -v_0^2 + c_2 - 1 \end{bmatrix} \begin{bmatrix} x_{ijkm}^{0100} \\ y_{ijkm}^{0100} \end{bmatrix} = \begin{bmatrix} p_{ijkm}^{0100} \\ q_{ijkm}^{0100} \end{bmatrix}, \quad (29)$$

$$(c_2 - v_0^2)z_{ijkm}^{0100} - 2v_0v_{ij-1km} = \tau_{ijkm}^{0100} + \eta d_{0000}x_{ijkm}^{0100} + \Lambda_{ij-1km}. \quad (30)$$

In this case, x_{ijkm}^{0100} and y_{ijkm}^{0100} can be solved directly. Λ_{ij-1km} represents the known term of v^2 of order $n - 1$. Letting $z_{ijkm}^{0100} = 0$, we have $v_{ij-1km} = -(\tau_{ijkm}^{0100} + \eta d_{0000}x_{ijkm}^{0100} + \Lambda_{ij-1km}) / 2v_0$.

Case 3: $(s, t, u, r) = (0, 0, 1, 0)$.

In this case, the undetermined coefficients should satisfy

$$\begin{bmatrix} \lambda_0^2 - 1 - 2c_2 & -2\sqrt{-1}\lambda_0 \\ -2\sqrt{-1}\lambda_0 & \lambda_0^2 + c_2 - 1 \end{bmatrix} \begin{bmatrix} x_{ijkm}^{0010} \\ y_{ijkm}^{0010} \end{bmatrix} + \begin{bmatrix} 2(\lambda_0 + \kappa_2)\lambda_{ijk-1m} \\ 2(\sqrt{-1}\kappa_2\lambda_0 - \sqrt{-1})\lambda_{ijk-1m} \end{bmatrix} = \begin{bmatrix} p_{ijkm}^{0010} \\ q_{ijkm}^{0010} \end{bmatrix} + \begin{bmatrix} \Gamma_{ijk-1m} \\ \sqrt{-1}\kappa_2\Gamma_{ijk-1m} \end{bmatrix}, \quad (31)$$

$$(c_2 + \lambda_0^2)z_{ijkm}^{0010} + 2\eta\kappa_3\lambda_0\lambda_{ijk-1m} = \tau_{ijkm}^{0010} + \eta d_{0000}x_{ijkm}^{0010} + \eta d_{ijk-1m} + \eta\kappa_3\Gamma_{ijk-1m}, \quad (32)$$

where Γ_{ijk-1m} represents the known term of λ^2 of order $n - 1$. Like the **Case 1**, by setting x_{ijkm}^{0010} to zero, the remaining terms y_{ijkm}^{0010} , z_{ijkm}^{0010} , and λ_{ijk-1m} can be computed correspondingly. More precisely, the reduced equations can be represented as

$$\begin{bmatrix} -2\sqrt{-1}\lambda_0 & 2(\lambda_0 + \kappa_2) \\ \lambda_0^2 + c_2 - 1 & 2(\sqrt{-1}\kappa_2\lambda_0 - \sqrt{-1}) \end{bmatrix} \begin{bmatrix} y_{ijkm}^{0010} \\ \lambda_{ijk-1m} \end{bmatrix} = \begin{bmatrix} p_{ijkm}^{0010} \\ q_{ijkm}^{0010} \end{bmatrix} + \begin{bmatrix} \Gamma_{ijk-1m} \\ \sqrt{-1}\kappa_2\Gamma_{ijk-1m} \end{bmatrix}, \quad (33)$$

$$(c_2 + \lambda_0^2)z_{ijkm}^{0010} = -2\eta\kappa_3\lambda_0\lambda_{ijk-1m} + \tau_{ijkm}^{0010} + \eta d_{ijk-1m} + \eta\kappa_3\Gamma_{ijk-1m}. \quad (34)$$

The corresponding undetermined coefficients can be obtained by solving the equations above.

2. Computation of the bifurcated orbits associating with the breaking of the S_2 -type symmetry

Associated with breaking of the S_2 -type symmetry, the iteration calculation procedure initiates with two coupling modification forms, coupling the motion either from the y -direction to the z -direction or vice versa. To avoid redundancy, we present the computation of undetermined coefficients for the first case in (19). Initializing with the modified linear solution (20), the undetermined coefficients are derived in an iterative process, with special treatments also applied to address the singular cases.

Case 1: $(s,t,u,r) = (1, 0, 0, 0)$.

Here, we can obtain the following linear equations:

$$\begin{bmatrix} -\omega_0^2 - 1 - 2c_2 & -2\omega_0 \\ -2\omega_0 & -\omega_0^2 + c_2 - 1 \end{bmatrix} \begin{bmatrix} x_{ijkm}^{1000} \\ y_{ijkm}^{1000} \end{bmatrix} + \begin{bmatrix} -2(\kappa_1 + \omega_0)\omega_{i-1jkm} \\ -2(1 + \kappa_1\omega_0)\omega_{i-1jkm} \end{bmatrix} = \begin{bmatrix} p_{ijkm}^{1000} \\ q_{ijkm}^{1000} \end{bmatrix} + \begin{bmatrix} \Omega_{i-1jkm} \\ \kappa_1\Omega_{i-1jkm} \end{bmatrix}, \quad (35)$$

$$(c_2 - \omega_0^2)z_{ijkm}^{1000} - 2\eta\omega_0\omega_{i-1jkm} = \tau_{ijkm}^{1000} + \eta d_{0000}y_{ijkm}^{1000} + \eta\kappa_1 d_{i-1jkm} + \eta\Omega_{i-1jkm}. \quad (36)$$

In this case, by letting y_{ijkm}^{1000} and z_{ijkm}^{1000} be zero, the system of linear equations become regular. The remaining coefficients can be obtained directly from the reduced linear equations.

Case 2: $(s,t,u,r) = (0, 1, 0, 0)$.

In this case, the coefficients can be computed by solving the following equations:

$$\begin{bmatrix} -v_0^2 - 1 - 2c_2 & -2v_0 \\ -2v_0 & -v_0^2 + c_2 - 1 \end{bmatrix} \begin{bmatrix} x_{ijkm}^{0100} \\ y_{ijkm}^{0100} \end{bmatrix} = \begin{bmatrix} p_{ijkm}^{0100} \\ q_{ijkm}^{0100} \end{bmatrix}, \quad (37)$$

$$(c_2 - v_0^2)z_{ijkm}^{0100} - 2v_0v_{ij-1km} = \tau_{ijkm}^{0100} + \eta d_{0000}y_{ijkm}^{0100} + \Lambda_{ij-1km}. \quad (38)$$

Here, x_{ijkm}^{0100} and y_{ijkm}^{0100} can be solved directly. Let $z_{ijkm}^{0010} = 0$. Then, the third equation (38) becomes solvable and the remaining coefficient v_{ij-1km} can be determined as $v_{ij-1km} = -\left(\tau_{ijkm}^{0100} + \eta d_{0000}x_{ijkm}^{0100} + \Lambda_{ij-1km}\right)/2v_0$.

Case 3: $(s,t,u,r) = (0, 0, 1, 0)$.

Similarly, the undetermined coefficients satisfy

$$\begin{bmatrix} \lambda_0^2 - 1 - 2c_2 & -2\sqrt{-1}\lambda_0 \\ -2\sqrt{-1}\lambda_0 & \lambda_0^2 + c_2 - 1 \end{bmatrix} \begin{bmatrix} x_{ijkm}^{0010} \\ y_{ijkm}^{0010} \end{bmatrix} + \begin{bmatrix} 2(\lambda_0 + \kappa_2)\lambda_{ijk-1m} \\ 2(\sqrt{-1}\kappa_2\lambda_0 - \sqrt{-1})\lambda_{ijk-1m} \end{bmatrix} = \begin{bmatrix} p_{ijkm}^{0010} \\ q_{ijkm}^{0010} \end{bmatrix} + \begin{bmatrix} \Gamma_{ijk-1m} \\ \sqrt{-1}\kappa_2\Gamma_{ijk-1m} \end{bmatrix}, \quad (39)$$

$$(c_2 + \lambda_0^2)z_{ijkm}^{0010} + 2\sqrt{-1}\eta\kappa_3\lambda_0\lambda_{ijk-1m} = \tau_{ijkm}^{0010} + \sqrt{-1}\eta\kappa_2 d_{ijk-1m} + \eta d_{0000}y_{ijkm}^{0010} + \sqrt{-1}\eta\kappa_3\Gamma_{ijk-1m}. \quad (40)$$

The singular algebraic equations mentioned above can be treated in a similar manner.

Except for these three special cases, the remaining undetermined coefficients in (23) can be obtained by solving the following regular system of linear equations:

$$\begin{bmatrix} -\tilde{\omega}_{stur}^2 - 1 - 2c_2 & -2\tilde{\omega}_{stur} \\ -2\tilde{\omega}_{stur} & -\tilde{\omega}_{stur}^2 + c_2 - 1 \end{bmatrix} \begin{bmatrix} x_{ijkm}^{stur} \\ y_{ijkm}^{stur} \end{bmatrix} = \begin{bmatrix} p_{ijkm}^{stur} \\ q_{ijkm}^{stur} \end{bmatrix}, \quad (41)$$

$$(c_2 - \tilde{\omega}_{stur}^2)z_{ijkm}^{stur} = \tau_{ijkm}^{stur} + \eta d_{0000}y_{ijkm}^{stur}. \quad (42)$$

IV. Results

In this section, we present a detailed quantitative analysis of pitchfork bifurcations around the collinear libration points in the ERTBP by tackling various parameterized bifurcation equations $\Delta(\eta, e, \alpha_1, \alpha_2, \alpha_3) = 0$. A detailed analysis for pitchfork bifurcations around the collinear libration points in the ERTBP is presented by tackling different parameterized bifurcation equations $\Delta(\eta, e, \alpha_1, \alpha_2, \alpha_3) = 0$ quantitatively. The emergence of non-zero solutions for η induces bifurcated orbits, including periodic/quasi-periodic orbits, hyperbolic orbits, and transit/non-transit orbits, whose explicit critical conditions are also derived.

A. Bifurcation associated with breaking of the S_1 -type symmetry

1. Solvability of the third-order bifurcation equation

From the previous section, we know that the S_1 -type symmetry breaking corresponding to a pitchfork bifurcation is induced by the coupling of motion in the x-direction to the z-direction. To analyze the specific bifurcation conditions, it is necessary to investigate the solutions of the bifurcation equation $\Delta = 0$. According to the linear equation for determining the coefficients d_{ijkm} in (27), the bifurcation equation has non-zero solutions $\eta(\alpha_1, \alpha_2, \alpha_3, e)$ provided when the trigonometric series solution (17) is computed up to the third order, i.e.,

$$\begin{aligned} \Delta &= d_{0000} + d_{2000}\alpha_1^2 + d_{0200}\alpha_2^2 + d_{0020}\alpha_3^2 + d_{0002}e^2 \\ &= a\eta^4 + b\eta^2 + c = 0, \end{aligned} \quad (43)$$

where $a = l_1\alpha_1^2 + l_2\alpha_3^2$, $b = l_3\alpha_1^2 + l_4\alpha_2^2 + l_5\alpha_3^2$, $c = l_6\alpha_1^2 + l_7\alpha_2^2 + l_8\alpha_3^2 + l_9e^2 + (\nu_0^2 - \omega_0^2)$. The coefficients l_i ($i = 1, 2, \dots, 9$) depend solely on the system parameter μ and their quantitative relationships are illustrated in Fig. 1. Here, the relatively negligible impact of the small orbital eccentricity on the bifurcation equation illustrates some

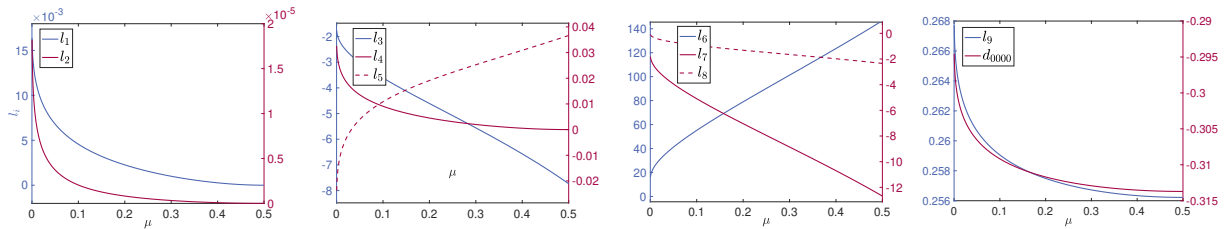


Fig. 1 Relationship between coefficients in the third-order bifurcation equation and the system parameter for L_1 in the ERTBP

significant similarities shared by the non-autonomous ERTBP and its approximated circular model from quantitative perspectives. By treating the bifurcation equation (43) as a quadratic equation in η^2 , a detailed bifurcation analysis can

be implemented as follows.

As previously discussed, the complex-valued amplitude α_3 which corresponds to the hyperbolic motion comprises two branches while one refers to non-transit trajectories (i.e. $\alpha_3 \in \mathbb{R}$) and the other branch describes the transit trajectories (i.e. $\alpha_3 \in \sqrt{-1}\mathbb{R}$). For the sake of simplicity, these two cases will be analyzed separately.

Case 1.1: $\alpha_3 \in \sqrt{-1}\mathbb{R}, c = 0, -\frac{b}{a} > 0$.

Replace the imaginary-valued amplitude α_3 with $\tilde{\alpha}_3 := \alpha_3/\sqrt{-1}$. Hereafter, α_3 will denote its real-valued counterpart. The critical surface $c = 0$ is then formulated as

$$c = l_6\alpha_1^2 + l_7\alpha_2^2 - l_8\alpha_3^2 + l_9e^2 + (\nu_0^2 - \omega_0^2) = 0. \quad (44)$$

For any $\mu \in (0, 0.5)$, the coefficients satisfy $l_6 > 0; l_7, l_8 < 0$. Now, (44) defines a one-sheet hyperboloid in the $(\alpha_1, \alpha_2, \alpha_3)$ coordinate system for any orbital eccentricity $0 < e < 1$. On the hyperboloid surface with condition $-b/a > 0$, there exist two distinct non-zero solutions given by $\eta = \pm\sqrt{-\frac{b}{a}}$. On the right side of the hyperboloid, four feasible η are obtained as

$$\eta = \pm\sqrt{\frac{-b \pm \sqrt{b^2 - 4ac}}{2a}}, \quad (45)$$

which solve the quadratic equation, while on the left side of the critical surface, the negativity of the coefficient c restricts the solutions to only two feasible values: $\eta = \pm\sqrt{\frac{-b + \sqrt{b^2 - 4ac}}{2a}}$.

Case 1.2: $\alpha_3 \in \sqrt{-1}\mathbb{R}, a = 0, -\frac{c}{b} > 0$.

In this case, the critical surface is represented as

$$a = l_1\alpha_1^2 - l_2\alpha_3^2 = 0. \quad (46)$$

On the critical surface, two distinct solutions $\eta = \pm\sqrt{-\frac{c}{b}}$ emerge. On the left part, there exist four feasible solutions, whereas on the other part, two solutions corresponding to (43) are given by $\eta = \pm\sqrt{\frac{-b + \sqrt{b^2 - 4ac}}{2a}}$.

It is noteworthy that both **Case 1.1** and **Case 1.2** suggest the occurrence of some potential bifurcations in hyperbolic part of the solution and, more generally, in transit and non-transit orbits. Unrevealed from the resonant bifurcation mechanisms, these newly identified bifurcated orbits in the ERTBP can now be systematically characterized through the parametrized bifurcation equation. Detailed descriptions of these orbits are provided in the subsequent subsections.

Case 1.3: $\alpha_3 \in \sqrt{-1}\mathbb{R}, b^2 - 4ac = 0, -\frac{b}{a} > 0$.

On the complicated critical surface defined by

$$(l_3\alpha_1^2 + l_4\alpha_2^2 - l_5\alpha_3^2)^2 - 4(l_1\alpha_1^2 - l_2\alpha_3^2)[l_6\alpha_1^2 + l_7\alpha_2^2 - l_8\alpha_3^2 + l_9e^2 + (\nu_0^2 - \omega_0^2)] = 0, \quad (47)$$

$\eta = \pm\sqrt{-\frac{b}{2a}}$ are the two feasible solutions corresponding to the bifurcation equation. Inside the surface, the condition $b^2 - 4ac < 0$ holds, indicating no bifurcation occurs in this region.

Fig. 2(a) illustrates these three critical cases as introduced above in the Sun-Earth system where the system parameter $\mu = 3.040423398444176e-6$ and the orbital eccentricity $e = 0.01671022$. The analytical analysis for the critical surfaces aligns with the distribution of feasible solutions of the third-order bifurcation in the case $\alpha_3 \in \sqrt{-1}\mathbb{R}$ as shown in Fig. 2(b).

Similarly, the solvability of (43) can be analyzed for amplitudes associated with non-transit orbits (i.e. $\alpha_3 \in \mathbb{R}$) in a manner analogous to the transit case. Specifically, the first critical surface is comparably defined as $\{(\alpha_1, \alpha_2, \alpha_3, e) \in \mathbb{R}^3 \times (0, 1) | c = 0, -\frac{b}{a} > 0\}$. In this case, the surface $c = 0$ describes a two-sheet hyperboloid in the $(\alpha_1, \alpha_2, \alpha_3)$ coordinate system, as shown in Fig. 2(c). Similar to **Case 1.1**, two additional feasible solutions, $\eta = \pm\sqrt{\frac{-b - \sqrt{b^2 - 4ac}}{2a}}$ emerge on the right side of the critical surface. For the non-transit case, the coefficient $a = l_1\alpha_1^2 + l_2\alpha_3^2$ is positive every where except at the origin, ensuring the degenerate case $\{(\alpha_1, \alpha_2, \alpha_3, e) \in \mathbb{R}^3 \times (0, 1) | a = 0, -c/b > 0\}$ does not exist. To conclude, the critical surface in non-transit case is illustrated in Fig. 2(c), while Fig. 2(d) presents the distribution of feasible solutions η .

2. Bifurcation analysis restricted to center manifolds

By setting $\alpha_3 = 0$ in (43), the reduced bifurcation equation can be expressed as

$$\Delta = \hat{a}\eta^4 + \hat{b}\eta^2 + \hat{c} = 0, \quad (48)$$

where $\hat{a} = l_1\alpha_1^2$, $\hat{b} = l_3\alpha_1^2 + l_4\alpha_2^2$, and $\hat{c} = l_6\alpha_1^2 + l_7\alpha_2^2 + l_9e^2 + (\nu_0^2 - \omega_0^2)$. In this case, the bifurcation curve in the (α_1, α_2) plane is defined by $\hat{c} = 0$. For any system parameter $\mu \in (0, 0.5)$ and a small orbital eccentricity e , the bifurcation curve

$$l_6\alpha_1^2 + l_7\alpha_2^2 = \omega_0^2 - \nu_0^2 - l_9e^2. \quad (49)$$

describes a hyperbola, as illustrated in Fig. 3(a), where two critical points $(\pm\sqrt{(\omega_0^2 - \nu_0^2 - l_9e^2)/l_6}, 0)$ lie on the α_1 -axis. When $\eta = 0$ and $\Delta \neq 0$, the series expansions (17) provide approximations to non-bifurcated orbits, encompassing Lyapunov orbits and Lissajous orbits. However, as α_1 and α_2 increase, non-zero solutions η to the bifurcation equation $\Delta = 0$ may emerge. These bifurcated solutions describe halo and quasi-halo orbits. Specifically, when $\alpha_2 = 0$, the series solutions with $\eta = 0$ represent the family of planar Lyapunov orbits. For $|\alpha_1| > \sqrt{(\omega_0^2 - \nu_0^2 - l_9e^2)/l_6}$, (48) yields a pair of non-zero solutions given by

$$\eta = \pm\sqrt{\frac{-l_3\alpha_1^2 - \sqrt{l_3^2\alpha_1^4 - 4l_1\alpha_1^2(l_6\alpha_1^2 + l_9e^2 + (\nu_0^2 - \omega_0^2))}}{2l_1\alpha_1^2}}, \quad (50)$$

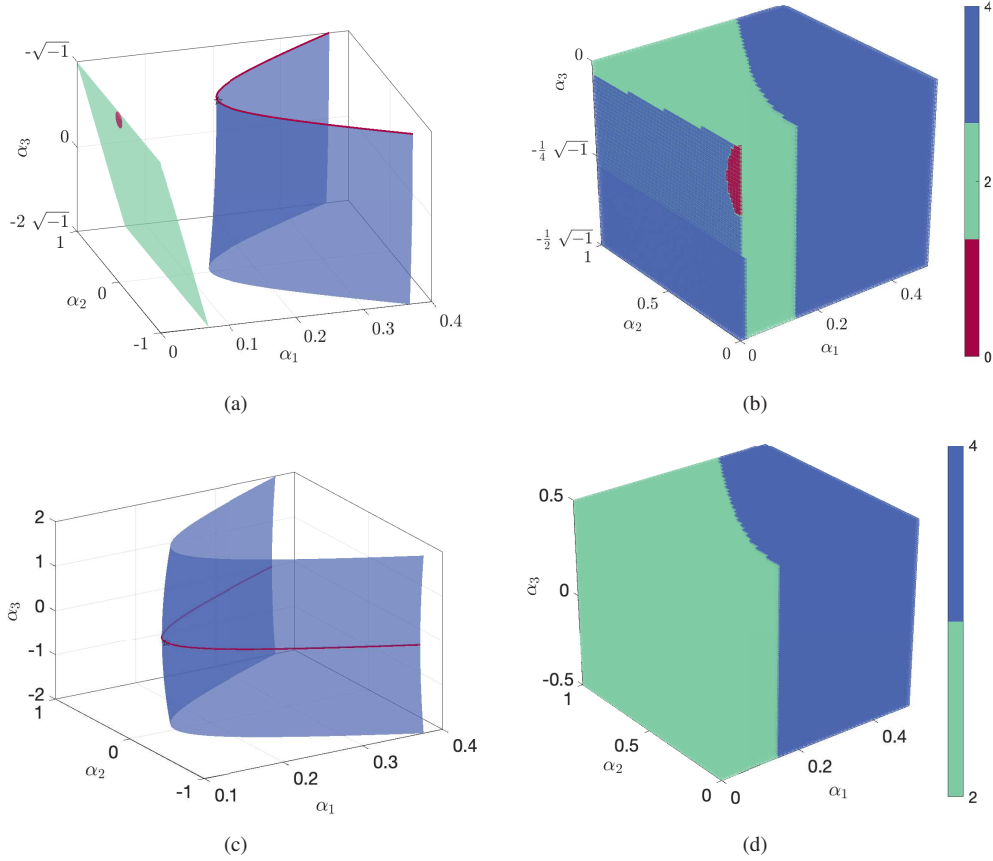


Fig. 2 Distribution of feasible solutions of the third-order bifurcation equation in the Sun-Earth system. (a) and (b): Critical surfaces and distribution of number of solutions η corresponding to transit orbits. (c) and (d): Critical surfaces and distribution of number of solutions η corresponding to non-transit orbits.

corresponding to the northern halo orbits and southern halo orbits respectively. When $\alpha_2 \neq 0$, Lissajous orbits are defined with $\eta = 0$, while quasi-halo orbits bifurcate from Lissajous orbits if $\eta \neq 0$ satisfies the bifurcation equation $\Delta = 0$. By using the Lindstedt-Poincaré method introduced in the preceding sections, here, the semi-analytical solution is computed up to the 7th order. Halo/quasi-halo orbits bifurcated from planar Lyapunov/Lissajous orbits around L_1 in the Sun-Earth ERTBP are shown in Fig. 3(b).

3. Bifurcation analysis of hyperbolic orbits

By letting the amplitudes corresponding to center part of (17), α_1, α_2 be zero, the bifurcation equation is simplified to

$$\Delta = l_2 \alpha_3^2 \eta^4 + l_5 \alpha_3^2 \eta^2 + l_8 \alpha_3^2 + l_9 e^2 + (v_0^2 - \omega_0^2) = 0. \quad (51)$$

When $\eta = 0$, $\Delta \neq 0$, no bifurcation occurs. In this case, (17) describes planar hyperbolic orbits. Bifurcated hyperbolic orbits emerge from these planar hyperbolic orbits when η is chosen as a non-zero solution to (51). Specifically, for

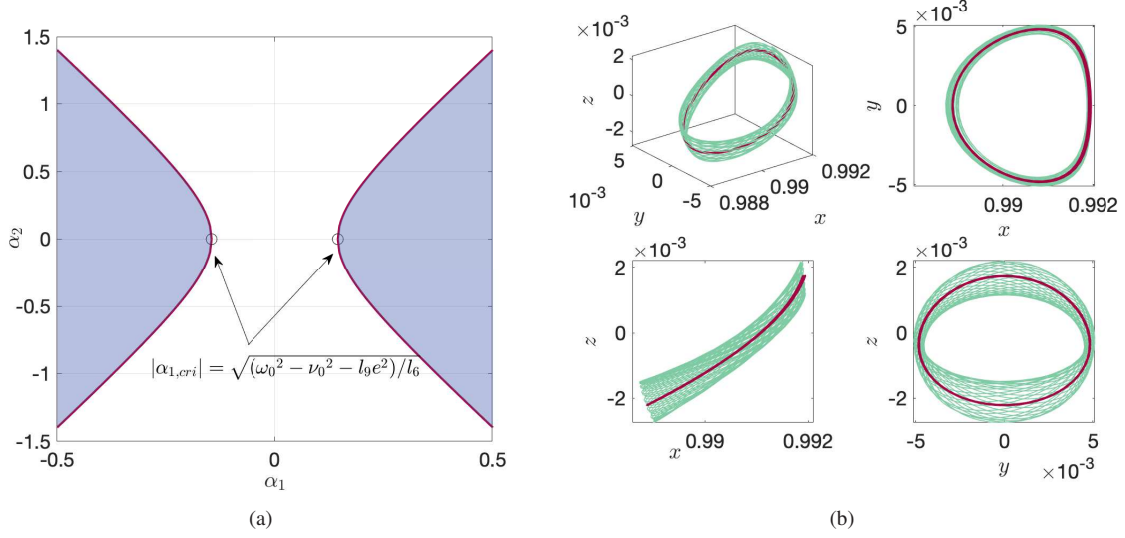


Fig. 3 (a): Bifurcation diagram of the third-order series solution of orbits in center manifolds associated with breaking of the S_1 -type symmetry. (b): Red: Halo orbit with $\alpha_1 = 0.15$. Green: Quasi-halo orbit with $\alpha_1 = 0.15$, $\alpha_2 = 0.04$.

$\alpha_3^2 > 0$, there exist a pair of real-valued η :

$$\eta = \pm \sqrt{\frac{-l_5 \alpha_3^2 + \sqrt{l_5^2 \alpha_3^4 - 4l_2 \alpha_3^2 [l_8 \alpha_3^2 + l_9 e^2 + (\nu_0^2 - \omega_0^2)]}}{2l_2 \alpha_3^2}}, \quad (52)$$

which solves the reduced bifurcation equation. Conversely, for $\alpha_3^2 < 0$ and $l_8 \alpha_3^2 + l_9 e^2 + (\nu_0^2 - \omega_0^2) > 0$, we can obtain up to four feasible solutions for (51), as seen in Fig. 4(a). Fig. 4(b) presents the bifurcated hyperbolic orbits that evolve beyond the (x, y) plane.

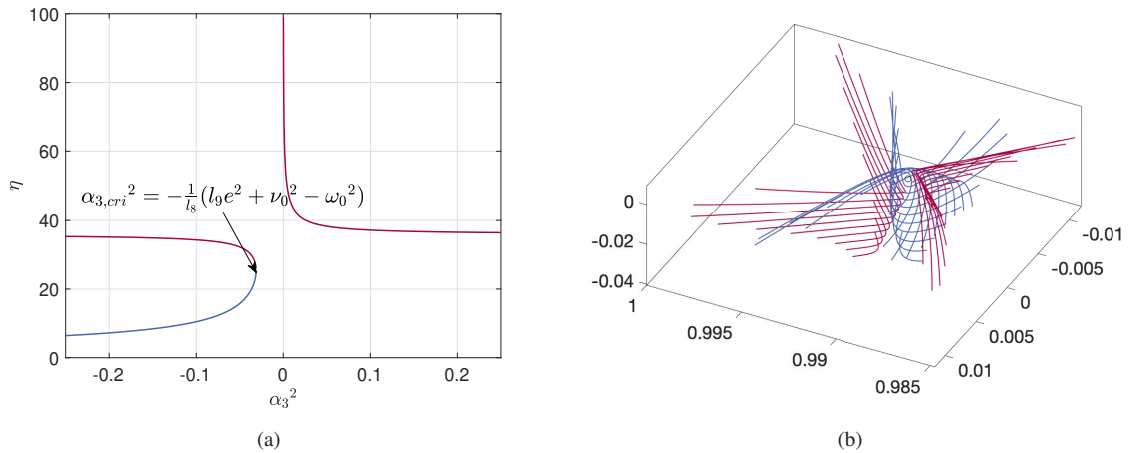


Fig. 4 (a): Positive solutions of the bifurcation equation with $\alpha_1 = \alpha_2 = 0$ corresponding to L_1 in the Sun-Earth system. (b): Hyperbolic orbits bifurcated from planar hyperbolic orbits.

4. Bifurcation analysis of transit/non-transit orbits

As previously discussed, when the amplitude α_3 associated with hyperbolic manifolds satisfies $\alpha_3 \in \sqrt{-1}\mathbb{R}$, the series solution (17) characterizes transit orbits in the ERTBP. Spacecraft can transit from one side of the collinear libration points to the other along these orbits. It is obtained from the bifurcation equation (51) that transit orbits also undergo bifurcations. Here, depending on different choices of feasible solutions η to $\Delta = 0$, we present two families of bifurcated transit orbits with different dynamical behaviors. Now, consider the case where $\alpha_1 \neq 0, \alpha_2 = 0$. When $\eta \neq 0$, It is observed that transit orbits bifurcate from planar orbits. Specifically, for relatively large values of η , the dynamics of the bifurcated transit orbits are primarily governed by motion in the hyperbolic direction. These orbits exhibit relatively rapid escape from the (x, y) plane. When η is selected from pairs with small absolute values $|\eta|$, an additional branch of bifurcated transit orbits (known as transit orbits of halo orbits in the ERTBP) emerges. In this scenario, the motion in the center part dominates, resulting in a slow variation of the z -axis. Fig. 5 illustrates the two distinct families of transit orbits bifurcated from planar orbits, highlighting the contrasting dynamical behaviors associated with different values of η .

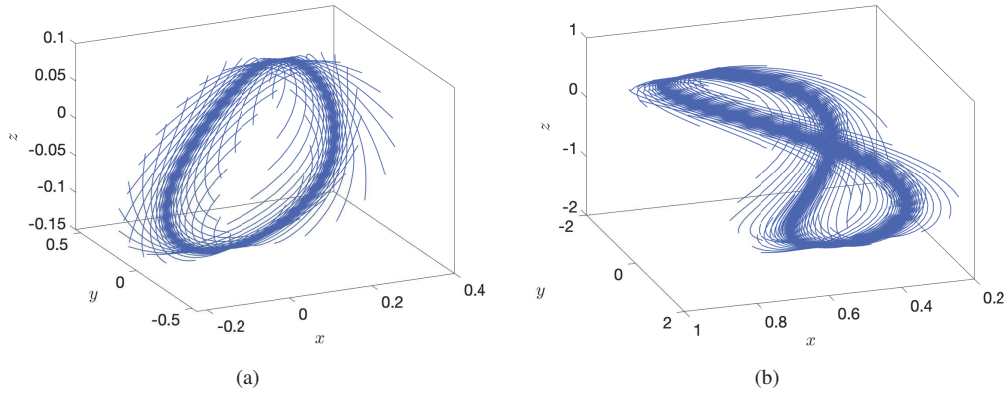


Fig. 5 Two branches of bifurcated transit orbits in the Sun-Earth system. (a) Transit orbits with $\alpha_1 = 0.15$, $\alpha_3 = \pm 0.005\sqrt{-1}$, $\eta = 0.7085$. (b) Transit orbits with $\alpha_1 = 0.15$, $\alpha_3 = \pm 0.005\sqrt{-1}$, $\eta = 9.4484$.

B. Bifurcation associated with the breaking of the S_2 -type symmetry

1. Case of coupling the motion in the z -direction to the motion in the y -direction.

In this case, the bifurcated solution first appears in the third-order series solution. The bifurcation equation is given by

$$\Delta = h_1\alpha_2^2\eta^2 + h_2\alpha_1^2 + h_3\alpha_2^2 + h_4\alpha_3^2 + h_5e^2 + \frac{1}{2\nu_0} - \frac{\nu_0}{2} = 0, \quad (53)$$

where h_i ($1 \leq i \leq 5$) depends solely on the system parameter μ . In the Sun-Earth system, the coefficients satisfy $h_2, h_3 > 0$, $h_4 < 0$. The critical surface determined by the bifurcation equation (53) is expressed as

$$h_2\alpha_1^2 + h_3\alpha_2^2 + h_4\alpha_3^2 + h_5e^2 + \frac{1}{2\nu_0} - \frac{\nu_0}{2} = 0. \quad (54)$$

When $\alpha_3 \in \mathbb{R}$, (54) describes a one-sheet hyperboloid in the $(\alpha_1, \alpha_2, \alpha_3)$ coordinates system, as shown in Fig. 6(a). When $\alpha_3 \in \sqrt{-1}\mathbb{R}$, replacing α_3 with its imaginary part $\alpha_3/\sqrt{-1}$, (54) describes an ellipsoid, as illustrated in Fig. 6(b). Setting $\alpha_3 = 0$, the critical surface (54) reduces to a critical curve in the (α_1, α_2) plane, as shown in Fig. 7(a), which

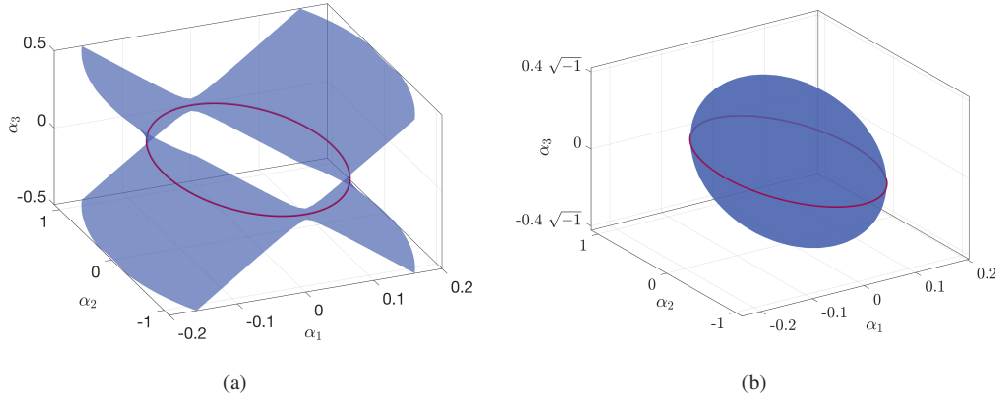


Fig. 6 Critical surfaces determined by the bifurcation equation for the case of considering a coupling effect from the motion in the z -direction to the y -direction. (a) Critical surface with α_3 associated with non-transit orbits. (b) Critical surface with α_3 associated with transit orbits.

illustrates the orbital bifurcation in center manifolds associated with the breaking of the S_2 -type symmetry. When the pair (α_1, α_2) lies outside the critical curve, (53) has no non-zero solution. In this case, the expansion (17) describes non-bifurcated Lyapunov orbits and Lissajous orbits. On the other hand, when (α_1, α_2) lies inside the critical ellipse, a pair of feasible solutions to the bifurcation equation exists, given by

$$\eta = \pm \sqrt{-\frac{1}{h_1\alpha_2^2} \left(h_2\alpha_1^2 + h_3\alpha_2^2 + h_5e^2 + \frac{1}{2\nu_0} - \frac{\nu_0}{2} \right)}, \quad (55)$$

which describes two families of axial orbits and their corresponding quasi-axial orbits. Specifically, two families of axial orbits bifurcate from vertical Lyapunov periodic orbits under the critical condition

$$|\alpha_2| \leq \sqrt{-\frac{1}{h_3} \left(h_5e^2 + \frac{1}{2\nu_0} - \frac{\nu_0}{2} \right)}. \quad (56)$$

The bifurcated axial/quasi-axial orbits in the Sun-Earth system are illustrated in Fig. 7(b).

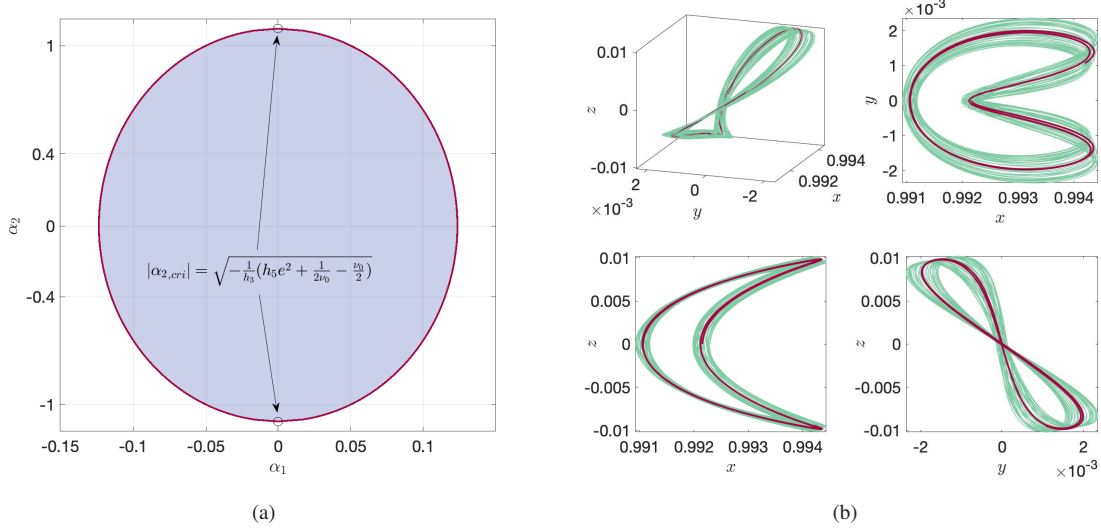


Fig. 7 (a): Bifurcation diagram of the third-order series solution of orbits in center manifolds in the case of coupling the motion in the z -direction to the motion in the y -direction. (b): Red: Axial orbit with $\alpha_1 = 0$, $\alpha_2 = 1$. Green: Quasi-halo orbit with $\alpha_1 = 0.005$, $\alpha_2 = 1$.

2. Case of coupling the motion in the y -direction to the motion in the z -direction.

It's obtained that axial/quasi-axial orbits can also bifurcate from planar Lyapunov periodic/Lissajous orbits. To demonstrate this, we consider the modification equations (19) which couples the motion in the y -direction to the motion in the z -direction. In this case, the bifurcation equation $\Delta = 0$ is initially formulated by

$$\Delta = (k_1\alpha_1^2 + k_2\alpha_3^2)\eta^4 + (k_3\alpha_1^2 + k_4\alpha_2^2 + k_5\alpha_3^2)\eta^2 + (k_6\alpha_1^2 + k_7\alpha_2^2 + k_8\alpha_3^2 + k_9e^2 + \frac{v_0^2 - \omega_0^2}{\kappa_1}) = 0, \quad (57)$$

where $k_i (1 \leq i \leq 9)$ depends solely on the system parameter μ . The critical surfaces in this case are illustrated in Fig. 8, similar to the case of coupling the motion in the x -direction to the z -direction. By letting the amplitude that associates with hyperbolic part of the solution be zero, the bifurcation equation (57) is reduced to

$$\Delta = k_1\alpha_1^2\eta^4 + (k_3\alpha_1^2 + k_4\alpha_2^2)\eta^2 + (k_6\alpha_1^2 + k_7\alpha_2^2 + k_9e^2 + \frac{v_0^2 - \omega_0^2}{\kappa_1}) = 0. \quad (58)$$

This equation defines a bifurcation curve in the (α_1, α_2) plane, as illustrated in Fig. 9(a). Similarly, feasible solutions η to the bifurcation equation (58) describe axial and quasi-axial orbits. In particular, when it satisfies that $\alpha_2 = \alpha_3 = 0$, and the absolute value of α_1 is smaller than some critical value given by

$$|\alpha_{1,cri}| = \sqrt{-\frac{1}{k_6}(k_9e^2 + \frac{v_0^2 - \omega_0^2}{\kappa_1})}, \quad (59)$$

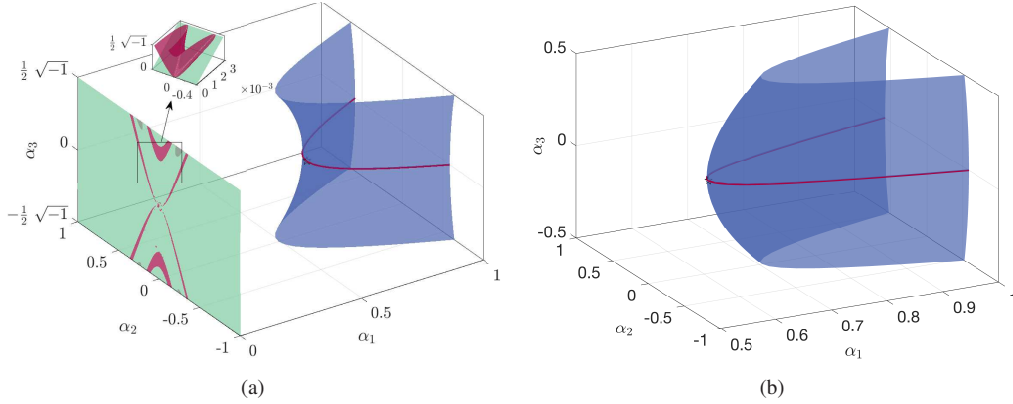


Fig. 8 Critical surfaces determined by the bifurcation equation for the case of considering a coupling effect from the motion in z -axis direction to the motion in the y -axis direction. (a) Critical surface with α_3 associated with transit orbits. (b) Critical surface with α_3 associated with non-transit orbits.

there exists a pair of feasible solutions η , satisfying

$$\eta = \pm \sqrt{\frac{-k_3\alpha_1^2 - \sqrt{k_3^2\alpha_1^4 - 4k_1\alpha_1^2(k_6\alpha_1^2 + k_9e^2 + \frac{\nu_0^2 - \omega_0^2}{\kappa_1})}}{2k_1\alpha_1^2}}. \quad (60)$$

These bifurcated solutions describe two families of axial orbits that bifurcate from planar Lyapunov orbits as shown in Fig. 9(b).

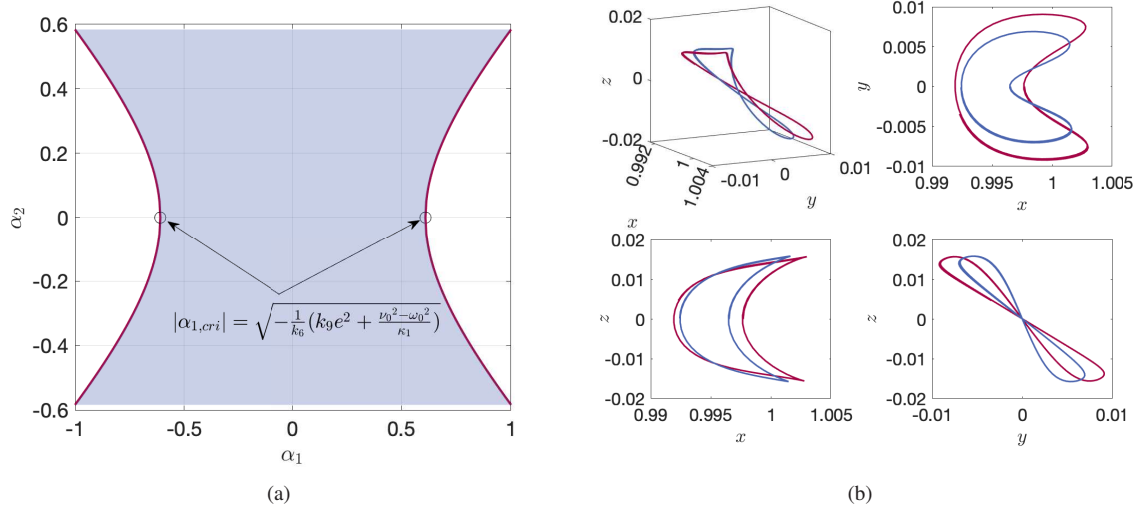


Fig. 9 (a): Bifurcation diagram of the third-order series solution of orbits in center manifolds in the case of coupling the motion in the z -direction to the motion in the y -direction. (b): Red: Axial orbit with $\alpha_1 = 0.28$. Blue: Axial orbit with $\alpha_1 = 0.2$.

V. Conclusions

In this paper, we present a semi-analytical framework to describe pitchfork bifurcations and symmetry breaking near collinear libration points in the ERTBP. By reformulating the hyperbolic components of the general solution within the complex field, we develop a unified trigonometric series-based approach to systematically exploit the inherent symmetries of the ERTBP. With the aid of coupling-induced bifurcation mechanisms, we achieve controlled symmetry breaking from the semi-analytical structures of non-bifurcated orbits. This is accomplished by constructing different bifurcation equations and introducing corresponding coupling coefficients that parametrize the transition between symmetric and asymmetric dynamical configurations. A quantitative study of these parametrized bifurcation equations reveals comprehensive insights into the intricate bifurcation dynamics triggered from pitchfork bifurcations in the non-autonomous ERTBP. Specifically, we demonstrate that the emergence of bifurcations is governed by the existence of feasible solutions ($\eta \neq 0$) to the bifurcation equation $\Delta = 0$, where solutions are determined solely by the orbital eccentricity e and three amplitude parameters α_i ($i = 1, 2, 3$). These bifurcations encompass not only periodic/quasi-periodic orbits but also transit/non-transit orbits, thereby unifying the characterization of bifurcations of both central and hyperbolic dynamical behaviors.

Acknowledgements

The author M.L. was partially supported by Sustainability Open Knowledge-Action Program by Connecting Multi-stakeholder Projects from Tohoku University.

Author Contributions

H.S. contributed to the methodology, software, validation, formal analysis, investigation and writing-original draft visualization. M.L. contributed to the conceptualization, software, writing-review and editing, supervision, project administration and funding acquisition.

Data Availability

The datasets generated during and analyzed during the current study are available from the corresponding author upon reasonable request.

Declarations

Conflict of interest The authors declare no conflict of interest.

References

- [1] Gómez, G., and Mondelo, J. M., “The dynamics around the collinear equilibrium points of the RTBP,” *Physica D: Nonlinear Phenomena*, Vol. 157, No. 4, 2001, pp. 283–321. [https://doi.org/10.1016/S0167-2789\(01\)00312-8](https://doi.org/10.1016/S0167-2789(01)00312-8).
- [2] Gómez, G., Masdemont, J. J., and Mondelo, J. M., *Libration point orbits: a survey from the dynamical point of view*, World-Scientific, Singapore, 2003, pp. 311–372. https://doi.org/10.1142/9789812704849_0016.
- [3] Broucke, R., “Stability of periodic orbits in the elliptic, restricted three-body problem,” *AIAA Journal*, Vol. 7, No. 6, 1969, pp. 1003–1009. <https://doi.org/10.2514/3.5267>.
- [4] Ovenden, M. W., and Roy, A. E., “On the use of the Jacobi integral of the restricted three-body problem,” *Monthly Notices of the Royal Astronomical Society*, Vol. 123, 1961, pp. 1–14. <https://doi.org/10.1093/mnras/123.1.1>.
- [5] Parker, J. S., and Anderson, R. L., *Low-energy lunar trajectory design*, John Wiley & Sons, Ltd, Hoboken, 2014. <https://doi.org/10.1007/s10569-012-9457-4>.
- [6] Peng, H., Bai, X. L., Masdemont, J. J., Gómez, G., and Xu, S. J., “Libration Transfer Design Using Patched Elliptic Three-Body Models and Graphics Processing Units,” *Journal of Guidance, Control, and Dynamics*, Vol. 40, No. 12, 2017, pp. 3155–3166. <https://doi.org/10.2514/1.G002692>.
- [7] Jorba-Cuscó, M., and Epenoy, R., “Low-fuel transfers from Mars to quasi-satellite orbits around Phobos exploiting manifolds of tori,” *Celest Mech Dyn Astr*, Vol. 133, No. 20, 2021. <https://doi.org/10.1007/s10569-021-10017-9>.
- [8] Shirobokov, M., Trofimov, S., and Ovchinnikov, M., “Survey of Station-Keeping Techniques for Libration Point Orbits,” *Journal of Guidance, Control, and Dynamics*, Vol. 40, No. 5, 2017, pp. 1085–1105. <https://doi.org/10.2514/1.G001850>.
- [9] Gurfil, P., and Meltzer, D., “Semi-Analytical method for calculating the elliptic restricted three-body problem monodromy matrix,” *Journal of Guidance, Control, and Dynamics*, Vol. 30, No. 1, 2007, pp. 266–271. <https://doi.org/10.2514/1.22871>.
- [10] Antoniadou, K. I., and Voyatzis, G., “2/1 resonant periodic orbits in three dimensional planetary systems,” *Celest Mech Dyn Astr*, Vol. 115, 2013, pp. 161–184. <https://doi.org/10.1007/s10569-012-9457-4>.
- [11] Peng, H., and Xu, S., “Stability of two groups of multi-revolution elliptic halo orbits in the elliptic restricted three-body problem,” *Celest Mech Dyn Astr*, Vol. 123, 2015, pp. 279–303. <https://doi.org/10.1007/s10569-015-9635-2>.
- [12] Ferrari, F., and Lavagna, M., “Periodic motion around libration points in the Elliptic Restricted Three-Body Problem,” *Nonlinear Dyn*, Vol. 93, No. 6, 2018, p. 453–462. <https://doi.org/10.1007/s11071-018-4203-4>.
- [13] Paez, R. I., and Guzzo, M., “Transits close to the Lagrangian solutions L_1 , L_2 in the elliptic restricted three-body problem,” *Nonlinearity*, Vol. 34, No. 9, 2021, pp. 6417–6449. <https://doi.org/10.1088/1361-6544/ac13be>.
- [14] Jorba, A., Nicolás, B., and Rodríguez, O., “A dynamical study of Hilda asteroids in the Circular and Elliptic RTBP,” *Chaos*, Vol. 34, No. 12, 2024. <https://doi.org/10.1063/5.0234410>.

- [15] Farquhar, R. W., “The Control and Use of Libration-Point Satellites,” Ph.D. thesis, Stanford Univ., Stanford, CA, 1969.
- [16] Richardson, D. L., “Analytic construction of periodic orbits about the collinear points,” *Celestial mechanics*, Vol. 20, No. 3, 1980, pp. 241–253. <https://doi.org/10.1007/BF01229511>.
- [17] Masdemont, J. J., “High-order expansions of invariant manifolds of libration point orbits with applications to mission design,” *Dynamical Systems*, Vol. 20, No. 1, 2005, pp. 59–113. <https://doi.org/10.1080/14689360412331304291>.
- [18] Jorba, A., and Masdemont, J. J., “Dynamics in the centre manifold of the collinear points of the Restricted Three Body Problem,” *Physica D: Nonlinear Phenomena*, Vol. 132, 1998. [https://doi.org/10.1016/S0167-2789\(99\)00042-1](https://doi.org/10.1016/S0167-2789(99)00042-1).
- [19] Paez, R. I., and Guzzo, M., “On the semi-analytical construction of halo orbits and halo tubes in the elliptic restricted three-body problem,” *Physica D: Nonlinear Phenomena*, Vol. 439, 2022. <https://doi.org/10.1016/j.physd.2022.133402>.
- [20] Celletti, A., Lhotka, C., and Pucacco, G., “The dynamics around the collinear points of the elliptic three-body problem: A normal form approach,” *Physica D: Nonlinear Phenomena*, Vol. 468, 2024. <https://doi.org/10.1016/j.physd.2024.134302>.
- [21] Lin, M., and Chiba, H., “Bifurcation Mechanism of Quasi-Halo Orbit from Lissajous Orbit,” *Journal of Guidance, Control, and Dynamics*, Vol. 48, No. 1, 2025. <https://doi.org/10.2514/1.G008233>.
- [22] Lin, M., Luo, T., and Chiba, H., “Semi-analytical computation of bifurcation of orbits near collinear libration point in the restricted three-body problem,” *Physica D: Nonlinear Phenomena*, Vol. 470, 2024. <https://doi.org/10.1016/j.physd.2024.134404>.
- [23] Doedel, E. J., Nomanov, V. A., Paffenroth, R. C., Keller, H. B., Dichmann, D. J., Galán-Vioque, J., and Vanderbauwhede, A., “Elemental periodic orbits associated with the libration points in the circular restricted 3-body problem,” *International Journal of Bifurcation and Chaos*, Vol. 17, No. 08, 2007, pp. 2625–2677. <https://doi.org/10.1142/S0218127407018671>.
- [24] Celletti, A., *Stability and chaos in celestial mechanics*, Springer Berlin, Heidelberg, 2010. <https://doi.org/10.1007/978-3-540-85146-2>.